INL/JOU-18-52171-Revision-0

Transformation of a ceramic precursor to a biomedical (metallic) alloy: Part I sinterability of Ta2O5 and TiO2 mixed oxides

January 2022

Prabhat K Tripathy, Maureen P. Chorney, Jerome P. Downey, Bridger P. Hurley, Kunal Mondal, Amey Rajendra Khanolkar

Changing the World's Energy Future

INL/JOU-18-52171-Revision-0

Transformation of a ceramic precursor to a biomedical (metallic) alloy: Part I sinterability of Ta2O5 and TiO2 mixed oxides

Prabhat K Tripathy, Maureen P. Chorney, Jerome P. Downey, Bridger P. Hurley, Kunal Mondal, Amey Rajendra Khanolkar

January 2022

Idaho National Laboratory
Idaho Falls, Idaho 83415

http://www.inl.gov

Prepared for the
U.S. Department of Energy
Under DOE Idaho Operations Office
Contract DE-AC07-05ID14517

Materials Science for Energy Technologies 5 (2022) 181–188

Contents lists available at ScienceDirect

Materials Science for Energy Technologies

journal homepage: www.keaipublishing.com/en/journals/materials-science-for-energy-technologies

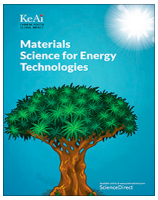

Transformation of a ceramic precursor to a biomedical (metallic) alloy: Part I – sinterability of Ta_2O_5 and TiO_2 mixed oxides

Maureen P. Chorney [a], Bridger P. Hurley [a], Kunal Mondal [b], Amey R. Khanolkar [b], Jerome P. Downey [a], Prabhat K. Tripathy [c,*]

[a] Department of Materials Science and Engineering, Montana Tech of the University of Montana, Butte, MT 59701, USA
[b] Materials Science and Engineering Department, Energy and Environment Science and Technology Directorate, Idaho National Laboratory, Idaho Falls, ID 83415, USA
[c] Pyrochemistry & Molten Salt Systems Department, Fuel Cycle Science and Technology Division, Nuclear Science and Technology Directorate, Idaho National Laboratory, Idaho Falls, ID 83415, USA

ARTICLE INFO

Article history:
Received 28 October 2021
Revised 22 January 2022
Accepted 22 January 2022
Available online 27 January 2022

Keywords:
Tantalum pentoxide
Titanium dioxide
Sintering
Phase evolution
Mixed oxides
Oxide morphology

ABSTRACT

Mixed Ta_2O_5 – TiO_2 binary system was studied by a combination of differential thermal analysis (DTA), scanning electron microscopy-energy dispersive spectrometry (SEM-EDS), X-ray diffraction (XRD) and *in situ* high temperature X-ray diffraction (HT-XRD) techniques. Different compositions of the mixed oxide powders were fabricated by ball–milling the powdered compositions, pelletizing the homogenized composite powders, and heating the green pellets in air at different temperatures for fixed time intervals. The sintered pellets were evaluated and characterized with respect to porosity, morphology, and phase distribution. DTA runs of the un-sintered powders indicated the onset temperatures for both exothermic and endothermic changes in the binary system. Significant amount of sintering was observed to take place at temperatures higher than 900 °C. Both room and high temperature X-ray diffraction patterns exhibited consistency in phase formation. A ternary compound ($TaTiO_4$) and a ternary solid solution ($Ti_{0.33}Ta_{0.67}O_2$) were observed to form in both room and high temperatures in addition to the respective binary phases (Ta_2O_5 and TiO_2). A sintering temperature in the range 900–1000 °C was observed to be adequate to achieve the requisite mechanical strength and optimum internal porosity (40–48%) for subsequent electrochemical polarization experiments.

1. Introduction

Among many alloying elements of titanium, tantalum is an excellent choice for biomedical applications because of its high degree of biocompatibility, corrosion resistance, good mechanical properties and high-strength-to-density ratio. Tantalum, being a beta stabilizer, shows superior properties with lower modulus as compared to either alpha or alpha and beta stabilized titanium alloys. That is why, in recent years, the binary tantalum - titanium (Ta-Ti) alloys, both in the bulk form and as a surface film on titanium, tantalum or on a suitable substrate, have evolved as superior biomaterials over either monolithic titanium or tantalum [1–5]. One of the extremely attractive properties of these alloys, among others, is their ductility as the binary system is not known to easily form intermetallic compounds and the ordering energies for these alloys are very low [6]. As compared to some of the other biomaterials, such as stainless steel, cobalt-chromium alloy, pure titanium, Ti-6Al-4 V alloy and pure tantalum, an alloy of titanium and tantalum (1:1 wt%) has demonstrated a higher strength-to-density ratio and an improved strength-to-modulus ratio, with an ultimate tensile strength of ~ 925 MPa and an elastic modulus of 75 GPa. Consequently, the binary titanium-tantalum alloys are being increasingly used as implants because of the twin combinations; improved corrosion resistance properties and excellent osseointegration characteristics [1–2]. In fact, it is the osseointegration property for which titanium-tantalum alloys are much in demand in the biomedical industry.

Although these alloys are endowed with attractive properties, their widespread use has been limited primarily because of the difficulties associated with their manufacturability. Use of titanium and tantalum powders to fabricate the alloy ingots by the special-

* Corresponding author.
E-mail address: Prabhat.Tripathy@inl.gov (P.K. Tripathy).
Peer review under responsibility of KeAi Communications Co., Ltd.

Production and hosting by Elsevier

https://doi.org/10.1016/j.mset.2022.01.006

ized melting techniques have made the widespread application of these alloys cost prohibitive. Besides these melting processes pose difficulties in terms of phase segregation and alloy homogenization. The phase segregation occurs due to a wide difference between their densities, 16.6 gcc^{-1} and 4.5 gcc^{-1} for tantalum and titanium respectively, which results in the segregation of elements during melt processing leading to alloy inhomogeneity [7]. In order to decrease the alloy inhomogeneity, the melting process is repeated several times. Also, because of their high melting points (Ta: 2996 °C and Ti: 1668 °C), the melting process itself is highly energy intensive. Besides, the very high melting point of tantalum may result in the loss of titanium by way of vaporization as the boiling point of titanium (3287 °C) is close to the melting temperature of tantalum. Currently, only specialized melting processes, such as vacuum arc melting, 3D laser engineering net shaping (LENS), selective laser melting techniques are used to fabricate these alloys [5,8–9]. Thus, there is a need to develop inexpensive manufacturing options for these as well as several other engineering alloys, widely used in energy and other critical sectors, such as defense, automotive, chemical processing, nuclear, to name a few.

In recent years, direct electrochemical reduction of metal oxides has been extensively studied to prepare many metals, including titanium and tantalum, and alloys [10–18]. Although a particular study reported the preparation of titanium-tungsten alloys from the mixed oxide precursors, the publication lacks data and information on the preparative aspects of the precursor materials [19]. As the preparation parameters of the oxide precursors critically influence the subsequent electrochemical polarization measurement (to prepare the constituent metals and alloys), it was decided to study the influence of the fabrication parameters on the mixed oxide precursor materials.

The Ta_2O_5 and TiO_2 mixed oxide precursor approach seems to offer a real possibility for its transformation to TiTa alloy by oxide polarization technique. A literature survey of TiO_2 and Ta_2O_5 indicates that both are important high-temperature materials and find many important applications, individually as well as in the mixed oxide form, in corrosion, electronics, structural materials, automotive, biomedical materials, chemical processing equipment, sensors, (photo) catalysis, and space industries. Some of the applications of the mixed oxide (Ta_2O_5-TiO_2) have been widely reported (i) for the fabrication of integrated circuit capacitors (because of the remarkable features of the composite oxide films, such as high dielectric strength, reduced leakage current and decreased breakdown voltage) [20] (ii) to prepare coatings for the interferometer mirrors used in current gravitational wave detectors [21] (iii) as photocatalytic devices in solar cells and high-laser induced damage threshold films [22–23] (iv) as the capacitor dielectrics in dynamic random access memory (DRAM) devices [24–25] and (v) as catalysts for the synthesis of chemicals, such as methanethiol from a mixture of H_2S and CO [26]. Quite a good number of studies have been reported pertaining to the synthesis and characterization of mixed oxide thin films with a view to improving the device functionality and phase stabilization (when added as a dopant, TiO_2 stabilizes the high temperature Ta_2O_5 phase). The individual oxides have a number of common features: (i) both exhibit polymorphism (ii) are good dielectric materials (Ta_2O_5 greatly enhances the dielectric constant of the TiO_2) (iii) can form protective surface coatings and as a result, resist corrosive attacks and (iv) exhibit reversible resistance switching phenomenon. Lagergren and Magneli have reported that Ta_2O_5 undergoes a phase transition at $\sim$ 1320 °C from the low-temperature phase (also known as L-Ta_2O_5 in the literature) to the high-temperature phase (H-Ta_2O_5) [27]. TiO_2 is known to have three different crystal structures: rutile (tetragonal), anatase and brookite. Determination of crystal structures of the high-temperature phase of Ta_2O_5 (H-Ta_2O_5) has been reported to be (i) orthorhombic [27] (ii) tetragonal [28] (iii) hexagonal and orthorhombic [29] (iv) one tetragonal, one monoclinic and one triclinic lattice structures [30] and (v) a combination of tetragonal, orthorhombic and monoclinic phases [31]. Unlike in the cases of individual Ta_2O_5 and TiO_2, the binary phase (Ta_2O_5-TiO_2) diagram has not been the subject matter of extensive investigation. Perhaps, Waring and Roth were the first to construct the binary phase diagram while they were studying the effect of TiO_2 doping on the polymorphism of Ta_2O_5 [30]. These authors have reported the formation of an equimolar ternary oxide ($TiTa_2O_7$) which was observed to melt at 1662 °C. They also postulated the existence of two other compounds ($\sim TiO_2$:49 Ta_2O_5 and TiO_2:7 Ta_2O_5). Further, they have reported that TiO_2 can accept a maximum of 9 mol% Ta_2O_5 in solid solution at 1630 °C and the binary system has two eutectic compositions, 31 and 54 mol% Ta_2O_5 with melting temperatures as 1630 °C and 1650 °C respectively. Ta^{5+} has a similar ionic radius with that of Ti^{4+} and hence readily dissolves in the TiO_2 lattice to form a series of substitutional alloys. Ta_2O_5 donates the electrons and as a result decreases the resistivity of TiO_2 [32].

The objective of the present research was therefore to develop a molten salt electrochemical process to prepare the binary alloy powders directly from the inexpensive mixed oxide precursors. Although formation of tantalum-tungsten alloy has been reported, no study has been reported on the preparation of titanium-tantalum alloy directly from the mixed oxide precursors. Therefore, the present study was undertaken to examine the feasibility of such a process**.** The electrochemical conversion of the mixed oxides to the alloy required the fabrication of the oxide precursor by a powder metallurgical process involving sintering of the powder mixture to design the oxide precursor with a set of desirable characteristics, such as percentage open porosity, oxide morphology, sintering atmosphere etc., prior to its electrochemical reduction. The present manuscript reports the first part of the experimental research pertaining to the preparation of the (mixed) oxide precursors for their subsequent electrochemical conversion to the tantalum-titanium (TaTi) alloys *in situ (*to be published as part II). The oxide precursors were prepared by ball-milling high purity Ta_2O_5 and TiO_2 powders, pelletizing the milled powder (to green pellets) and sintering them at elevated temperatures for fixed durations. The sinterability, phase formation and % porosity in the sintered oxides were determined by differential thermal analysis, X-ray diffraction and Archimedes principle respectively. Another highlight of the present work was the recording of the *in situ* high-temperature XRD data during the sintering process.

2. Experimental

2.1. Materials

High-purity and finely powdered Ta_2O_5 (Sigma Aldrich 99.99%, trace metals basis, < 44 μm) and TiO_2, (J.T. Baker, AR grade, <44 μm) were used as the start materials. Poly(ethylene glycol) (PEG, Sigma-Aldrich, average MW = 200) and poly(vinyl butyral-co-vinyl alcohol-co-vinyl acetate) (PVB/PVA, Sigma-Aldrich, average MW = 50,000–80,000 by GPC) were added as the binders to the mixed oxides during the milling stage.

2.2. Preparative method

The powder mixture (with the binders) was homogenized by way of preparing a slurry in isopropyl alcohol (91%). The mixed slurry was ball-milled for a duration of 12 h to ensure homogenization of the contents. The homogenized powder was then pelletized, in a 13 mm dia. steel die, under a laboratory hydraulic press by applying a pressure in the range 31.0–33.1 MPa.

2.3. Instruments/Equipment

The green pellets were placed in an alumina boat and heated, both in air and under hydrogen flow, in an MTI 1100X series furnace to the desired temperature for different durations. The initial characterization of the mixed powder was carried out in a TGA-DSC (SDT Q600 Series) set up. The sintered pellets were evaluated and characterized, with respect to phase distribution and morphological features, by powder X-ray diffraction (Rigaku Ultima IV diffractometer with PDXL software) and SEM-EDS SEM (TESCAN MIRA3 with an EDS attachment) techniques. High-temperature X-ray diffraction (HT-XRD) patterns were recorded by attaching the furnace to the Rigaku diffractometer and heating the mixed powders to the desired temperatures. The samples were prepared on a platinum stage to minimize the effects of thermal expansion on the samples. A heating rate of 10 °C/min was employed to achieve the set temperature. The samples were held at the predetermined temperatures for about five minutes before recording the diffraction patterns.

3. Results and discussion

3.1. TG-DTA characterization of the sintering behavior

On the basis of phase diagram, proposed by Waring and Roth [30], three compositions (mol%) ($45Ta_2O_5$ – 55 TiO_2, $50Ta_2O_5$ – $50TiO_2$ and $55Ta_2O_5$ – $45TiO_2$) were selected to prepare and characterize the mixed oxide precursors. All the three compositions were heated, in air atmosphere, up to a maximum temperature of 1150 °C. Out of these three compositions, two ($45Ta_2O_5$ – $55TiO_2$ and $55Ta_2O_5$ – $45TiO_2$) were observed to exhibit pronounced DTA peaks (Figs. 1 and 2 respectively), which perhaps indicated the formation of possible chemical interactions. The appearance of broad exotherms in the temperature ranges ~ 770–1000 °C could have been due to the disordering of metal atoms, crystallization, phase change(s) or rapid grain growth. As expected, both the thermogravimetric analysis (TGA) patterns recorded insignificant weight losses (1.88 wt% and 1.33 wt% respectively). Fig. 1 also indicated a very broad DTA peak in the temperature range ~ 800–1000 °C. On the other hand, the $55Ta_2O_5$ – $45TiO_2$ indicated possible chemical interactions at comparatively lower temperatures (~773 °C and 982 °C respectively). On the basis of these DTA patterns, bulk samples, with both compositions, were prepared. The green pellets were sintered at two different sets of temperatures (825 °C and 1000 °C for the $45Ta_2O_5$ – $55TiO_2$ mixture and 625 °C and 900 °C for the $55Ta_2O_5$ – $45TiO_2$ composition) in order to examine their sintering behaviors. Unlike in the case of both 45 Ta_2O_5-55 TiO_2 and $55Ta_2O_5$-45 TiO_2 compositions, the 50:50 composition didn't show any significant sintering behavior up to a temperature of 1050 °C and as a result was not chosen as a possible composition for the fabrication of the mixed oxide precursor.

3.2. Phase analysis by room-temperature XRD

3.2.1. $45Ta_2O_5$ – $55TiO_2$ (mol%) composition

Except for the formation of a tiny amount of a ternary phase ($TiTaO_4$), the X-ray diffraction pattern of the pellet, prepared at 825 °C (in air), did not show the formation of any major mixed (ternary) oxide phase. The major phases were tantalite (43.8% Ta_2O_5), rutile (36.74%, TiO_2) and anatase (12.02%, TiO_2) (Table 1).

Besides $TiTaO_4$, the pellet, sintered at 1000 °C (in air), showed the formation of a minor solid solution phase ($Ti_{0.33}Ta_{0.67}O_2$) (Table 2). Also, a sharp drop in the anatase phase content (from 12.02 at 825 °C to 1.2 at 1000 °C) was observed at higher sintering temperature. The major phases were just Ta_2O_5 (43.8%) and TiO_2 (rutile, 37.1%) respectively.

The two ternary phases, described by Equations (1) and (2), together accounted for the 13.4% phase composition (Table 2).

$$Ta_2O_5(s) + 2TiO_2(s) = 2TiTaO_4(s) + 0.5O_2(g) \quad (1)$$

$$Ta_2O_5(s) + TiO_2(s) = 3Ti_{0.33}Ta_{0.67}O_2(s) + 0.5O_2(g) \quad (2)$$

3.2.1.1. $55Ta_2O_5$-$45TiO_2$ (mol%) composition. The pellet, sintered at 625 °C, was analyzed to have three major phases: tantalite (64.8%), rutile (12.07%) and anatase (11.47%) (Table 3).

The three minor phases consisted of two mixed oxides and a solid solution phase and together they formed 9.7% of the total phases. The combined fraction of the rutile and anatase phases

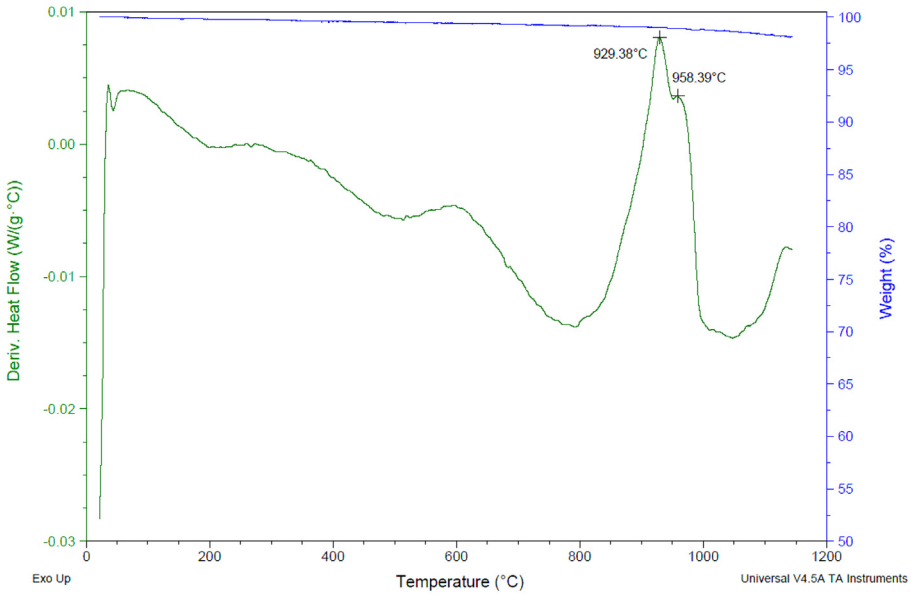

Fig. 1. TG- DTA scan of the mixed oxide powder ($45Ta_2O_5$ – 55 TiO_2, mol%), powder amount – 8.444 mg, blue line: TGA and green line: DTA trace. (For interpretation of the references to colour in this figure legend, the reader is referred to the web version of this article.)

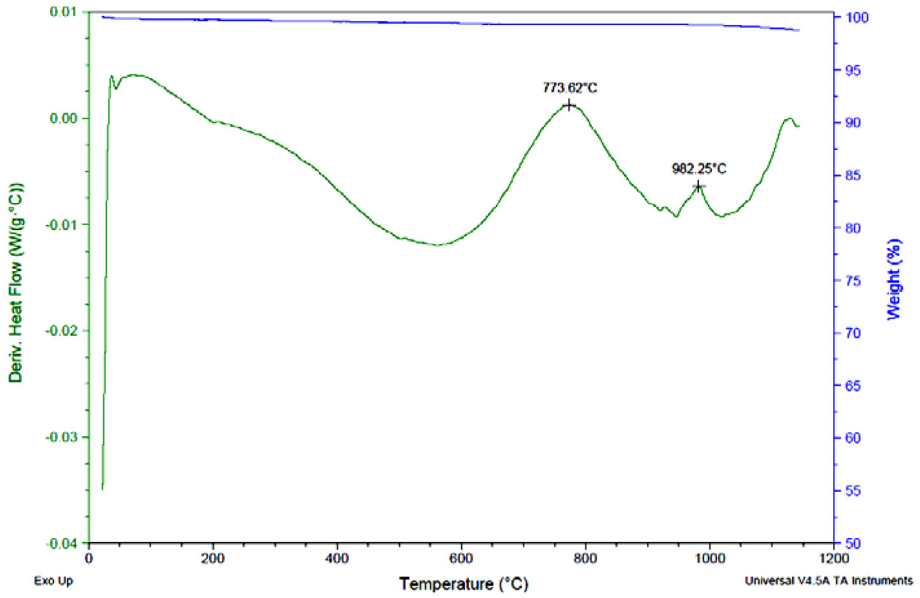

Fig. 2. TG-DTA scan for the $55Ta_2O_5$-$45TiO_2$ (mol.%) sample (sample weight – 8.886 mg).

Table 1
Phase analysis of the $45Ta_2O_5$-$55TiO_2$ pellet sintered at 825 °C by room temperature XRD.

Phase	Formula	Figure of Merit (FOM) value	Card No	Amount (wt. %)	Total $Ta_xTi_yO_z$
Tantite, syn	Ta_2O_5	0.615	01–089-2843	43.79	
Anatase	TiO_2	1.098	01–071-1169	12.02	
Rutile HP, syn	TiO_2	2.333	01–071-4513	36.74	
Struverite, syn	$TaTiO_4$	3.664	01–071-0929	3.48	
Titanium (III) Tantalum Oxide	$TaTiO_4$	3.165	01–081-0912	3.97	
				100.0	7.45

Table 2
Phase analysis of the $45Ta_2O_5$-$55TiO_2$ pellet sintered at 1000 °C by room temperature XRD.

Phase	Formula	Figure of Merit (FOM) value	Card No	Amount (wt.%)	Total $Ta_xTi_yO_z$
Tantalum Oxide	Ta_2O_5	0.704	01–070-9177	48.24	
Anatase	TiO_2	1.470	01–071-1169	1.20	
Rutile HP, syn	TiO_2	3.338	01–071-4513	37.11	
Titanium Tantalum Oxide	$(Ti_{0.33}Ta_{0.67})O_2$	1.776	01–085-0103	3.51	
Titanium (III) Tantalum Oxide	$TiTaO_4$	3.099	01–081-0912	9.93	
				99.99	13.44

Table 3
Phase analysis of the $55Ta_2O_5$-$45TiO_2$ pellet sintered at 625 °C (in air) by room temperature XRD.

Phase	Formula	FOM	Card No	Amount (wt.%)	Total $Ta_xTi_yO_z$
Tantalite, syn	Ta_2O_5	0.623	01–089-2843	64.79	
Anatase, syn	TiO_2	0.838	01–084-1285	11.47	
Rutile HP, syn	TiO_2	3.957	01–071-4513	12.07	
Struverite	$TiTaO_4$	2.209	01–071-0929	3.02	
Titanium Tantalum Oxide	$(Ti_{0.33}Ta_{0.67})O_4$	1.567	01–085-0103	2.62	
Titanium (III) Tantalum Oxide	$TiTaO_4$	3.073	01–081-0912	6.04	
				100.01	9.68

Table 4
Phase analysis of the $55Ta_2O_5$-$45TiO_2$ pellet sintered at 900 °C (in air) by room temperature XRD.

Phase	Formula	FOM	Card No	Amount (wt. %)	Total $Ta_xTi_yO_z$
Tantalite, syn	Ta_2O_5	0.536	01–089-2843	75.6	
Anatase, syn	TiO_2	1.015	01–084-1285	11.4	
Rutile HP, syn	TiO_2	4.036	01–071-4513	3.00	
Struverite	$TiTaO_4$	3.53	01–071-0929	4.00	
Titanium (III) Tantalum Oxide	$TiTaO_4$	1.702	01–081-0912	6.00	
				100.00	10.0

was observed to be lower as compared to the fractions observed in the $45Ta_2O_5$-$55TiO_2$ composition. At 900 °C, two mixed oxide (and no solid solution) phases were formed (Table 4) and the total content of the mixed phases was marginally higher than that formed at 625 °C (Table 4).

Waring and Roth's binary phase diagram [30] has reported the formation of three phases: low-temperature Ta_2O_5 (L-Ta_2O_5, postulated to occur at ~ $7Ta_2O_5$:TiO_2) and a mixed oxide phase ($TiTa_2O_7$) for compositions between ~ 12–50 mol%Ta_2O_5 up to a temperature ~ 1200 °C. At temperatures higher than 1200 °C and in the same composition ranges, they have reported the formation of a solid solution, high temperature Ta_2O_5 phase (H-Ta_2O_5) and one mixed oxide phase ($TiTa_2O_7$). At a concentration higher than 50 mol%Ta_2O_5, and up to a temperature of 1200 °C, the phases consisted of a TiO_2 solid solution and the mixed oxide phase ($TiTa_2O_7$). Finally, at concentrations < ~ 12 mol% Ta_2O_5, they have reported the formation of multiple phases that include triclinic (metastable) Ta_2O_5 solid solution, monoclinic (metastable) Ta_2O_5, triclinic (metastable) Ta_2O_5 and tetragonal Ta_2O_5, L-Ta_2O_5 (with approximately two compositions, 49 Ta_2O_5:TiO_2 and $7Ta_2O_5$:TiO_2) in the temperature range 100–1200 °C. In another investigation, Brennecka and Payne have reported the formation of a porous microstructure with $8TiO_2.92Ta_2O_5$ composition by sintering the mixed oxides at 1400 °C for 24 h. These authors have also reported that the addition of TiO_2 to Ta_2O_5 resulted in the reduction of the densification temperature of the composite ceramics, which, in turn, hindered phase transformation of the L-Ta_2O_5 to H-Ta_2O_5 [33]. Unlike their studies, the present studies have reported the formation of two different mixed oxide phases, $(Ti_{0.33}Ta_{0.67})O_2$ and $TiTaO_4$ respectively. The absence of the stoichiometric mixed oxide ($TiTa_2O_7$) and other phases, reported by Waring and Roth, can perhaps be explained by the fact that these authors adopted an elaborate and sequential heating schedule to prepare the samples at higher temperatures than the temperatures used in the present studies. In the first stage, they heated the mixtures of TiO_2 and Ta_2O_5 at 1000 °C for 16 h which was followed up by another heating cycle at higher temperatures (1400–1657 °C) for durations ranging from 2 to 264 h [29] to improve the diffusion kinetics. As the objective, in the present study, was to achieve some degree of sinterability prior to the electrochemical reduction of the mixed oxide to form the binary alloys, a longer duration heating cycle, to observe the formation of different oxide phases, was not adopted.

3.3. Phase evolution in the mixed oxides (high-temperature X-ray diffraction)

With a view to examining the dynamic phase evolution, in the mixed oxides, both the $45Ta_2O_5$ – $55TiO_2$ (mol.%) and 55 Ta_2O_5 – 45 TiO_2 (mol.%) compositions were subjected to high-temperature X-ray diffraction studies. Calculated quantities of high-purity and fine-grained mixed oxide (Ta_2O_5 and TiO_2) powders were placed on a platinum stage, to minimize the effects due thermal expansion, and the mixture was subjected to heating (in air) up to a maximum temperature of 1000 °C at a heating rate of 10°Cmin^{-1}. The samples were held for 5 min., at each temperature, prior to recording the respective diffraction patterns using a scintillation counter. The X-ray diffractrograms were recorded at different temperatures. Tables 5 and 6 show the quantitative phase analyses data for both the compositions.

3.3.0.1. 45 Ta_2O_5 – 55 TiO_2 composition

As expected, XRD patterns recorded in the temperature range 30–1000 °C looked identical (Table 3). However, the quantitative phase analysis indicated a gradual increase in the formation of the mixed oxides up to a temperature of ~ 930 °C (Table 5). Further increase in temperature to 1000 °C resulted in a decrease in the mixed oxide contents (Table 5). The quantitative analysis performed on the five diffractograms indicates a large increase in the formation of mixed oxides as the temperature of the sample is increased from 825 °C to 930 °C (only 6.07 % mixed oxide versus

Table 5
Quantitative analysis results (WPF) for the 45 Ta_2O_5 – $55TiO_2$ (mol.%) system, obtained from the high temperature XRD diffractograms.

Temp. (°C)	Phase	Formula	FOM	Card No	Content	Total $Ta_xTi_yO_z$
30	Tantalum Oxide	Ta_2O_5	0.670	01–070-9177	78.58	
	Anatase	TiO_2	0.913	01–071-1167	14.41	
	Rutile HP, syn	TiO_2	1.969	01–071-4513	7.01	
					100.00	
825	Tantalum Oxide	Ta_2O_5	0.572	01–070-9177	52.74	
	Anatase	TiO_2	0.733	01–071-1167	7.36	
	Rutile HP, syn	TiO_2	2.344	01–071-4513	33.83	
	Struverite, syn	$TiTaO_4$	3.072	01–071-0929	1.00	
	Titanium (III) Tantalum Oxide	$TiTaO_4$	2.025	01–081-0912	3.48	
	Titanium Tantalum Oxide	$(Ti_{0.33}Ta_{0.67})O_2$	3.142	01–085-0103	1.59	
					100.00	6.07
930	Tantalum Oxide	Ta_2O_5	0.580	01–070-9177	49.54	
	Anatase	TiO_2	0.743	01–071-1167	9.49	
	Rutile HP, syn	TiO_2	2.199	01–071-4513	9.99	
	Struverite, syn	$TiTaO_4$	2.251	01–071-0929	21.98	
	Titanium (III) Tantalum Oxide	$TiTaO_4$	3.195	01–081-0912	4.00	
	Titanium Tantalum Oxide	$(Ti_{0.33}Ta_{0.67})O_2$	2.553	01–085-0103	5.00	
					100.00	30.98
960	Tantalum Oxide	Ta_2O_5	0.558	01–070-9177	59.46	
	Anatase	TiO_2	0.723	01–071-1167	10.51	
	Rutile HP, syn	TiO_2	3.261	01–071-4513	1.00	
	Struverite, syn	$TiTaO_4$	2.341	01–071-0929	20.02	
	Titanium (III) Tantalum Oxide	$TiTaO_4$	3.740	01–081-0912	6.01	
	Titanium Tantalum Oxide	$(Ti_{0.33}Ta_{0.67})O_2$	3.038	01–085-0103	3.00	
					100.00	29.03
1000	Tantalum Oxide	Ta_2O_5	0.557	01–070-9177	55.40	
	Anatase	TiO_2	0.577	01–071-1167	11.30	
	Rutile HP, syn	TiO_2	1.914	01–071-4513	12.00	
	Struverite, syn	$TiTaO_4$	2.410	01–071-0929	16.00	
	Titanium (III) Tantalum Oxide	$TiTaO_4$	3.764	01–081-0912	5.30	
					100.00	21.30

Table 6
Quantitative analysis results (WPF) for the 55 Ta_2O_5 – 45TiO_2 (mol.%) system, obtained from the high temperature XRD diffractograms.

Temp. (°C)	Phase	Formula	FOM	Card No	Content	Total $Ta_xTi_yO_z$
625	Tantalum Oxide	Ta_2O_5	0.462	01–070-9177	44.98	10.04
	Anatase	TiO_2	0.695	01–071-1168	6.83	
	Rutile HP, syn	TiO_2	1.809	01–071-4513	38.15	
	Struverite, syn	$TiTaO_4$	1.626	01–071-0929	6.02	
	Titanium Tantalum Oxide	$(Ti_{0.33}Ta_{0.67})O_2$	2.785	01–085-0103	4.02	
					100.00	
775	Tantalum Oxide	Ta_2O_5	0.457	01–070-9177	53.95	
	Anatase	TiO_2	0.890	01–071-1167	5.92	
	Rutile HP, syn	TiO_2	1.809	01–071-4513	9.03	
	Struverite, syn	$TiTaO_4$	2.379	01–071-0929	19.06	
	Titanium (III) Tantalum Oxide	$TiTaO_4$	2.200	01–081-0912	12.04	
					100.00	31.10
928	Tantalum Oxide	Ta_2O_5	0.517	01–070-9177	72.94	
	Anatase	TiO_2	0.698	01–071-1167	5.81	
	Rutile HP, syn	TiO_2	2.117	01–071-4513	8.02	
	Struverite, syn	$TiTaO_4$	3.623	01–071-0929	9.22	
	Titanium Tantalum Oxide	$Ti_{0.33}Ta_{0.67}O_2$	2.608	01–085-0103	4.01	
					100.00	13.23
983	Tantalum Oxide	Ta_2O_5	0.539	01–070-9177	51.60	
	Anatase	TiO_2	0.911	01–071-1167	5.49	
	Rutile HP, syn	TiO_2	2.302	01–071-4513	34.93	
	Struverite, syn	$TiTaO_4$	3.360	01–071-0929	7.98	
					100.00	7.98
1000	Tantalum Oxide	Ta_2O_5	0.603	01–070-9177	52.58	
	Anatase	TiO_2	1.091	01–071-1167	5.75	
	Rutile HP, syn	TiO_2	3.303	01–071-4513	33.73	
	Titanium (III) Tantalum Oxide	$TiTaO_4$	3.821	01–081-0912	6.94	
	Titanium Tantalum Oxide	$Ti_{0.33}Ta_{0.67}O_2$	3.840	01–085-0103	1.00	
					100.00	7.94

30.98 % mixed oxide). The high percentage of mixed oxide present was maintained through 960 °C, but the increase of temperature to 1000 °C caused a slight decrease resulting in the sample containing 21.30 % mixed oxides.

No sintering was observed to take place at a temperature<100 °C for both the compositions. Formation of a solid solution ($Ti_{0.33}Ta_{0.67}O_2$) and mixed oxides (two forms of $TiTaO_4$) were seen in the two compositions and their quantities were observed to be maximum at 775 °C (31.1%) and 930 °C (30.98%) for 55Ta_2O_5-45TiO_2 and 45Ta_2O_5-55TiO_2 compositions respectively (Tables 5 and 6). No definite phase formation patterns were observed in both the compositions. For example, in the 45Ta_2O_5-55TiO_2 composition, the solid solution phase was observed at a comparatively higher temperature (825 °C) than that seen in the 55Ta_2O_5-45TiO_2 mixture (625 °C). Similarly, this phase was not observed at 1000 °C in the 45Ta_2O_5-55TiO_2 mixture but was present in the composition containing higher amounts of Ta_2O_5. Another notable observation was the effect of pelletization. While pelletization resulted in higher fractions of mixed oxides at comparatively lower temperatures, 900 °C (55Ta_2O_5 – 45TiO_2) and 825 °C (45Ta_2O_5 – 55TiO_2) respectively, both the compositions at 1000 °C showed relatively lesser amounts of the mixed oxide phases.

Both room and high temperature X-ray diffractograms indicated consistency in terms of the formation of possible phases in the binary Ta_2O_5-TiO_2 system.

4. Morphology of the sintered pellets

Morphological features of the sintered pellets were examined under a scanning electron microscope. Fig. 3 shows the microstructure of the 45Ta_2O_5-55TiO_2 (mol.%) prepared at 825 °C and 1000 °C respectively.

Sintering temperature, among other parameters such as particle size distribution, pelletization pressure, sintering additives, sintering duration etc. influences the morphology of the sintered products. Temperature, in general, has been observed to profoundly influence

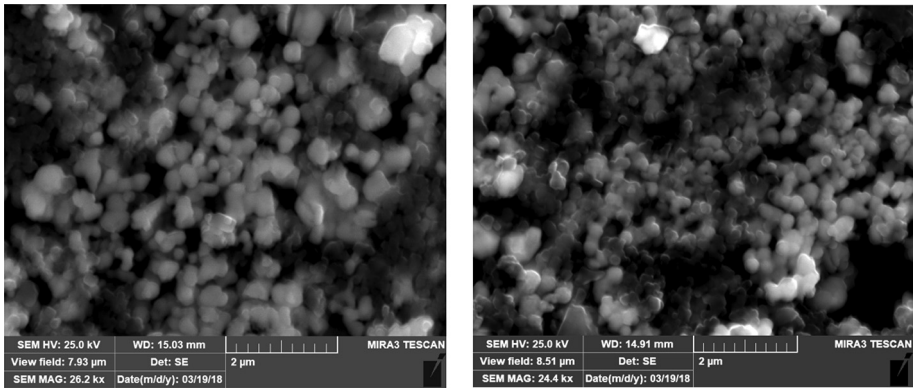

Fig. 3. Fig. 3: SEM images of 45 Ta_2O_5 – 55 TiO_2 sintered at 825 °C in air (left) and 1000 °C (right). White (jagged) pieces were due to the aluminum contamination during ball milling operation.

the microstructure of the sintered body. Too high a temperature can result in extensive necking and/or significant grain growth resulting in the formation of a very dense microstructure. Similarly, a low temperature may not be adequate to sinter the particles and impart mechanical rigidity. Such a scenario will not be able to hold the oxide particles together during the reduction process.

As can be seen from the Fig. 3, a sintering temperature of 825 °C was inadequate to achieve good sinterability of the mixed oxides. On the other hand, the pellet sintered at 1000 °C showed definite signs of necking and particle growth. As expected, the sintered pellet, prepared at 1000 °C, was observed to have a reduced porosity compared to that prepared at 825 °C. However, a slight reduction in porosity at 1000 °C did not affect the overall reduction efficiency of the pellet to form the binary alloy.

Fig. 4 shows the morphology of the $55Ta_2O_5$-$45TiO_2$, sintered at two different temperatures (625 °C and 900 °C respectively). As can be seen from the microphotographs, the pellet sintered at 900 °C showed somewhat better sintering behavior. Lower temperature heating (625 °C and 825 °C) did not result in good sintering as is evident from the formation of more granular particles after sintering (Figs. 3 and 4). These pellets were also observed to crack and break into pieces during subsequent handling. The pellets, prepared at 890 °C and 1000 °C, were observed to have better strength for their subsequent electrochemical conversion to binary alloys.

5. Sintered pellet porosity

The presence of porosity in sintered ceramic bodies is often not preferred for certain applications and the objective is to achieve the density as close to the theoretical density. However, in the present study a sintered pellet with certain degree of porosity proved beneficial from the standpoint of achieving better oxygen removal kinetics during its subsequent polarization in the fused salt. Too high a porosity (~80%) resulted in the disintegration of the sintered pellet, in the fused salt. A relatively lower porosity (<10%) was observed to have incomplete electrochemical reduction. A porosity in the range 30–50% resulted in the formation of better-quality alloys. A combination of 900/1000 °C sintering temperature and 2 h of sintering duration (for the green bodies) in air yielded an open porosity in the range 40–48% (Fig. 5), which proved to be adequate for the formation of the binary alloys (Fig. 6). A monolithic

Fig. 6. Reduced TaTi powder, prepared from the pellet $45Ta_2O_5$-$55TiO_2$ (air-sintered): electrolyte – $CaCl_2$-1% CaO; polarization temperature: 950 °C; polarization duration: 36 h; cell potential: 2.5–3.1 V; counter electrode – 3 mm dia. and 100 mm long ruthenium rod.

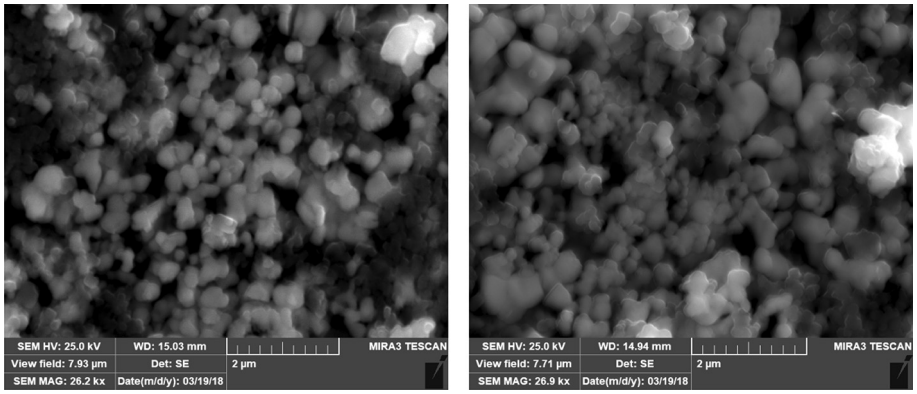

Fig. 4. SEM images of $55Ta_2O_5$ – $45TiO_2$ sintered in air at 625 °C (left) and 900 °C (right).

Fig. 5. Air-sintered pellets: (left): 45 Ta_2O_5-$55TiO_2$ (1000 °C/2h) and (right): $55Ta_2O5$-$45TiO_2$ (900 °C/2h). The respective porosities were 40% and 48% respectively.

platinum group metal anode [34–35], for the electrochemical conversion of the sintered bodies (Fig. 5) to the constituent alloy powders (Fig. 6), proved to be highly beneficial in terms of rendering the overall alloy manufacturing process environmentally friendly.

6. Conclusions

Sintering and phase evolution behavior in the binary Ta_2O_5 and TiO_2 mixed oxide system were studied at different temperatures. Simultaneous TG-DTA analysis yielded composition-dependent thermograms. Although thermograms indicated some chemical interactions at an onset temperature as low as ~ 625 °C, significant sintering could only be observed at a relatively higher temperature (900 °C). Both room as well as high temperature X-ray diffraction patterns revealed the formation of limited mixed oxide and solid solution phases when two specific mixed powder compositions, 45 mol%Ta_2O_5 – 55 mol%TiO_2 and 55 mol%Ta_2O_5 – 45 mol%TiO_2 respectively, were heated in air up to a maximum temperature of 1000 °C for a duration of 4 h. The green (sintered) pellets, prepared at 900 °C and 1000 °C, were observed to have adequate mechanical integrity and percentage open porosity (in the range 40–48%) for their subsequent electrochemical transformation to alloy powders.

Declaration of Competing Interest

The authors declare that they have no known competing financial interests or personal relationships that could have appeared to influence the work reported in this paper.

Acknowledgement

The work was supported by the Idaho National Laboratory Directed Research and Development Program under DOE Idaho Operations Office. The manuscript was authorized by Battelle Energy Alliances under the contract No. DE-AC07-05ID14517, with the US Department of Energy, for publication. The US government retains and the publisher, by accepting the manuscript for publication, acknowledges that the US government retains a non-exclusive, paid up irrevocable worldwide license to publish or reproduce the published form of this manuscript or allow others to do so for United States Government purposes.

References

[1] K. Prasad, O. Bazaka, M. Chua, M. Rochford, L. Fedrick, J. Spoor, R. Symes, M. Tieppo, C. Collins, A. Cao, D. Markwell, K (Ken). Ostrikov, K. Bazaka, Metallic biomaterials: current challenges and opportunities, Materials 10 (8) (2017) 884, https://doi.org/10.3390/ma10080884.

[2] Y.-L. Zhou, M. Niinomi, T. Akahori, M. Nakai, H. Fukui, Comparison of various properties between Ti-Ta alloy and pure Ti for biomedical applications, Mater. Trans. 48 (3) (2007) 380–384.

[3] E. Eisenbarth, D. Velten, M. Mueller, R. Thull and J. Breme, "Biocompatibility of β-stabilizing elements of titanium alloys", **25**, 26 (2004) 5705-13.

[4] H. Prigent, P. Pellen-Mussi, G. Cathelineau, M. Bonnaure-Mallet, Evaluation of the biocompatibility of titanium-tantalum alloy versus titanium, J. Biom. Mater. Res.: Off. J. Soc. Biomater. Jpn. Soc. Biomater. Aust. Soc. Biomater. 39 (2) (1998) 200–206.

[5] S. Huang, S.L. Sing, G. de Looze, R. Wilson, W.Y. Yeong, Laser powder bed fusion of titanium-tantalum alloys: compositions and designs for biomedical applications, J. Mech. Behav. Biomed. Mater. 108 (2020) 103775, https://doi.org/10.1016/j.jmbbm.2020.103775.

[6] T. Chakraborty, J. Rogal, R. Drautz, Martensitic transformation between competing phases in Ti-Ta Alloys: a solid-state nudged elastic band study, J. Physics: Condens. Matter. 27 (11) (2015) 115401, https://doi.org/10.1088/0953-8984/27/11/115401.

[7] A. Morita, H. Fukui, H. Tadano, S. Hayashi, J. Hasegawa, M. Niinomi, Alloying titanium and tantalum by cold crucible levitation melting (CCLM) furnace, Mater. Sci. Eng. **A** 280 (1) (2000) 208–213.

[8] S.L. Sing, W.Y. Yeong, F.E. Wirla, Selective laser melting of titanium alloys with 50 wt.% tantalum: microstructure and mechanical properties, J. Alloys Compounds 660 (2016) 461–470.

[9] J. Fuerst, D. Medlin, M. Carter, J. Sears, G. Vander Voort, Laser additive manufacturing of titanium-tantalum alloy structured interfaces for modular orthopedic devices, J. Metals 67 (4) (2015) 775–780.

[10] G.Z. Chen, D.J. Fray, T.W. Farthing, Direct electrochemical reduction of titanium dioxide to titanium in molten calcium chloride, Nature 407 (6802) (2000) 361–364.

[11] K.S. Mohandas, "Direct electrochemical conversion of metal oxides to metal by molten salt electrolysis: a review", Mineral Processing and Extractive Metallurgy, 5, Trans. Inst. Mining Metallur.: Sect. C 122 (4) (2013) 195–212.

[12] J.i. Zhao, S. Lu, L. Hu, C. Li, Nano Si preparation by constant cell voltage electrolysis of FFC-Cambridge Process in molten $CaCl_2$, J. Energy Chem. 22 (6) (2013) 819–825.

[13] D. Tang, H. Yin, X. Cheng, W. Xiao, D. Wang, Green production of nickel powder by electro-reduction of NiO in molten Na_2CO_3–K_2CO_3, Int. J. Hydrogen Energy 41 (41) (2016) 18699–18705.

[14] A.M. Abdelkader, D.J. Fray, Direct electrochemical preparation of Nb–10Hf–1Ti alloy, Electochim. Acta 55 (8) (2010) 2924–2931.

[15] R. Bhagat, M. Jackson, D. Inman, R. Dashwood, The production of Ti–Mo alloys from mixed oxide precursors via the FFC Cambridge process, J. Electrochem. Soc. 155 (6) (2008) E63–E69.

[16] R. Barnett, K.T. Kilby, D.J. Fray, Reduction of tantalum pentoxide using graphite and tin-oxide-based anodes via the FFC-Cambridge process, Metallur. Mater. Trans. 40 (2) (2009) 150–157.

[17] C. Schwandt, G.R. Doughty, D.J. Fray, The FFC Cambridge process for Ti metal winning, Key Eng. Mater. 436 (2010) 13–25.

[18] R. Bhagat, M. Jackson, D. Inman, R.J. Dashwood, Production of Ti-W alloys from mixed oxide precursors via the FFC Cambridge process, J. Electrochem. Soc. 156 (1) (2008) E1–E7.

[19] R.J. Howell, L.A. Benson Marshall, M. Jackson, B.P. Wynne, P. Villechaise, B. Appolaire, P. Castany, M. Dehmas, C. Delaunay, J. Delfosse, A. Denquin, E. Gautier, L. Germain, N. Gey, T. Gloriant, J.-Y. Hascoët, S. Hémery, Y. Millet, D. Monceau, F. Pettinari-Sturmel, M. Piellard, F. Prima, B. Viguier, A Method for the Production of Titanium-Tantalum Binary Alloys Using the Metalysis-FFC Process, MATEC Web Conf. 321 (2020) 07012, https://doi.org/10.1051/matecconf/202032107012.

[20] M.C. Nielson, J.-Y. Kim, E.J. Rymaszewski and T.-M. Lu, "Low temperature deposition of high dielectric films using reactive pulsed DC magnetron sputtering", in W.D. Brown, S.S. Ang, M. Loboda, B. Sammakia, R. Singh and H.S. Rathore (Eds.), Dielectric material integration for microelectronics, The Electrochemical Society Proceedings Series, USA, Proc. Vol. **98-3**, 1998, pp. 227-40.

[21] T. Damart, E. Coillet, A. Tanguy, D. Rodney, Numerical study of structural and vibrational properties of amorphous Ta_2O_5 and TiO_2-doped Ta_2O_5, J. Appl. Phys. 119 (2016) 175106.

[22] A. Krishnaprasanth, M. Seetha, Solvent free synthesis of Ta_2O_5 nanoparticles and their photocatalyic properties, Am. Inst. Phys. Adv. 8 (2018) 055017.

[23] C. Xu, D. Lin, J.-N. Niu, Y.-H. Qiang, D.-W. Li, C.-X. Tao, Preparation of Ta-doped TiO_2 using Ta_2O_5 as the doping source, Chin. Phys. Lett. 32 (8) (2015) 088102.

[24] Q. Fang, C. Hodson, M. Liu, Z.W. Fang, R. Potter, R. Gunn, Preliminary investigation of high-k materials – TiO_2 doped Ta_2O_5 films by remote plasma ALD, Phys. Proc. 32 (2012) 379–388.

[25] Y. Wang, Y.-J. Jiang, Composition dependence of dielectric properties of $(Ta_2O_5)_{1-x}(TiO_2)_x$ polycrystalline ceramics, Mat. Sci. and Eng. B 99 (1–3) (2003) 221–225.

[26] Y. Chen, J.L.G. Fierro, T. Tanaka, I.E. Wachs, Supported tantalum oxide catalysts: synthesis, physical characterization, and methanol oxidation chemical probe reaction, J. Phys. Chem. B 107 (2003) 5243–5250.

[27] S. Lagergren, A. Magnéli, A.E. Nielsen, J. Plíva, J.S. Sörensen, N.A. Sörensen, On the tantalum-oxygen system, Acta Chem. Scand. 6 (1952) 444–446.

[28] A.I. Zaslavskii, R.A. Zvinchuk, A.G. Tutov, X-ray studies of Ta_2O_5 polymorphism, Dokl. Akad. Nauk SSSR 104 (1955) 409–411.

[29] E.E. Nikishina, E.N. Lebedeva, D.V. Drobot, Niobium – and tantalum – containing oxide materials: synthesis, properties and application, Inorg. Mater. 48 (13) (2012) 1243–1260.

[30] J.L. Waring, R.S. Roth, "Effect of oxide additions on the polymorphism of tantalum pentoxide system Ta_2O_5-TiO_2", J. Research of the National Bureau of Standards – A, Phys. Chem. 72A (2) (1968) 175–186.

[31] X.Q. Liu, X.D. Han, Z. Zhang, L.F. Ji, Y.J. Jiang, The crystal structure of high temperature phase Ta_2O_5, Acta Mater. 55 (7) (2007) 2385–2396.

[32] M.R.D. Bomio, V.C. Sousa, E.R. Leite, J.A. Varela, E. Longo, Nonlinear behavior of TiO_2.Ta_2O_5.MnO_2 material doped with BaO and Bi_2O_3, Mater. Chem. Phys. 85 (1) (2004) 96–103.

[33] G.L. Brennecka, D.A. Payne, Densification and grain growth for powder-derived Ta_2O_5-TiO_2 ceramics, J. Ceramic Soc. Jpn. 115 (1346) (2007) 678–682.

[34] P.K. Tripathy, K. Mondal, A.R. Khanolkar, One-step manufacturing process for neodymium-iron (magnet-grade) master alloy, Mater. Sci. Energy Technol. 4 (2021) 249–255.

[35] P.K. Tripathy, "Electrochemical cells for direct oxide reduction and related methods", U.S. Patent (US10,872,705B2, December 22, 2020).